Climate Dynamics
https://doi.org/10.1007/s00382-018-4275-3

Role of topography on the MJO in the maritime continent: a numerical case study

Haochen Tan[1] · Pallav Ray[1] · Bradford S. Barrett[2] · Mukul Tewari[3] · Mitchell W. Moncrieff[4]

Received: 21 November 2017 / Accepted: 19 May 2018

Abstract
The role of topography on a Madden–Julian Oscillation (MJO) event in the Maritime Continent (MC) is explored using a regional model. Four simulations are conducted: lower-resolution (12 km) simulations using cumulus parameterization in the presence (LR) and absence (LR-Flat) of topography, and higher-resolution (4 km) simulations without cumulus parameterization in the presence (HR) and absence (HR-Flat) of topography. In the LR simulation, the MJO remains unorganized with no clear eastward propagation, while the LR-Flat simulation captures the MJO and its eastward propagation across the MC. In the absence of cumulus parameterization, both HR and HR-Flat capture the MJO and show several similarities and differences compared to the LR and LR-Flat simulations. To better understand these differences, a moisture budget analysis is conducted during the passage of the MJO. In the LR-Flat simulation, vertical advection of moisture is increased to the east of the islands, leading to continuity in MJO-associated convection, continuity that was not present in the LR simulation. The increase in vertical advection in the absence of topography is due to an increase in the mean moisture advection by the anomalous vertical winds. In the middle of the MC, horizontal advection seems to be the most important for an uninterrupted eastward propagation of the MJO. The increase in the horizontal advection in the absence of topography is primarily due to an increase in the anomalous moisture advection by the mean zonal winds. To what extent the MJO was influenced by the upstream effect from the New Guinea topography was also explored. These results indicate that the important physical processes for MJO-associated convection may be different in different parts of the MC. Further implications of these results in the context of other recent studies on MJO propagation across the MC are discussed.

Keywords Madden–Julian oscillation · Maritime continent · Topography · High-resolution

1 Introduction

The Maritime Continent (MC) is the largest archipelago in the world (Fig. 1a). Ramage (1968) introduced the term "Maritime Continent" and recognized the region as one of the primary heat sources for global atmospheric circulation (e.g., Meehl 1987; Keenan et al. 1989; Neale and Slingo 2003; Keenan and Carbone 2008; Moncrieff et al. 2012a; Peatman et al. 2014). The MC is bounded by the Pacific and Indian Oceans to east and west, respectively, and is part of the Indo-Pacific warm pool. Because of the warm sea surface temperatures (SSTs), deep convection is abundant, and it is further enhanced by the region's complex topography. The mountainous islands in the MC can induce strong land-sea breeze circulations, and hence precipitation over the major islands (Yang and Slingo 2001; Mori et al. 2004; Ichikawa and Yasunari 2006, 2008).

This paper is a contribution to the special issue on Advances in Convection-Permitting Climate Modeling, consisting of papers that focus on the evaluation, climate change assessment, and feedback processes in kilometer-scale simulations and observations. The special issue is coordinated by Christopher L. Castro, Justin R. Minder, and Andreas F. Prein.

✉ Haochen Tan
htan2013@my.fit.edu

[1] Florida Institute of Technology, Melbourne, FL 32904, USA

[2] US Naval Academy, Annapolis, MD, USA

[3] IBM, T.J. Watson Research Center, New York, USA

[4] National Center for Atmospheric Research, Boulder, CO, USA

Published online: 26 May 2018

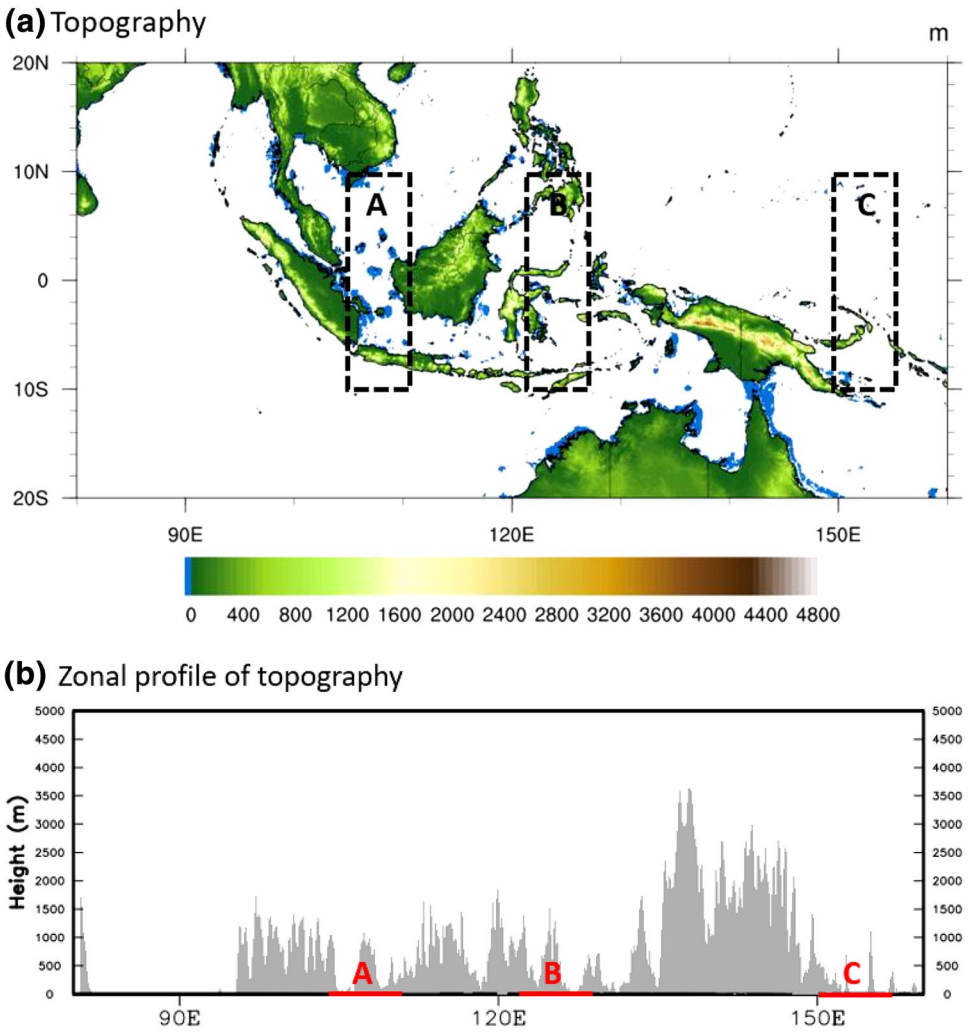

Fig. 1 **a** Topography (m) and **b** Zonal (10°S–10°N) profile of maximum terrain height (m) in the Maritime Continent. The top panel also indicates the domain (80°–160°E, 20°S–20°N) of the model simulations. The three dashed boxes marked as A, B, and C in top panel are the three areas chosen for detailed analysis when the MJO propagates across these areas. Area A (105°–111°E, 10°S–10°N) is located to the east of Sumatra, Area B (122°–128°E, 10°S–10°N) is to the east of Borneo and Sulawesi, and Area C (150°–156°E, 10°S–10°N) is at the eastern edge of the MC. The longitudinal extents of the three areas are also marked in the bottom panel. The terrain height is from the Global Digital Elevation Model (ETOPO2) dataset from National Geophysical Data Center (NGDC)

The Madden–Julian oscillation (MJO; Madden and Julian 1971; Zhang 2005), a dominant mode of intraseasonal (20–100 day) variability in the tropics, propagates eastward along the equator with a speed of about 5 m s^{-1}. Previous studies have demonstrated that when the MJO propagates across the MC, it is influenced by the MC in different ways (e.g., Inness et al. 2003; Sobel et al. 2010; Oh et al. 2013; Feng et al. 2015; Hagos et al. 2016; Kim et al. 2017; Zhang and Ling 2017) including the complex topography of the islands (Hsu and Lee 2005; Wu and Hsu 2009). In a recent study, Tseng et al. (2017) found that topography may distort the coupled Kelvin–Rossby wave structure (e.g., Rui and Wang 1990), and concluded that past studies based on aqua-planet framework (e.g., Ajayamohan et al. 2013) may have provided an oversimplified view of the MJO. Inness and Slingo (2006) also concluded that blocking of Kelvin waves by topography could contribute to MJO weakening in the MC. This leads to unrealistic simulations in coarse-resolution models that poorly represent the topography (Inness and Slingo 2006; Wang et al. 2014; Peatman et al. 2015).

Apart from the large-scale structures of the MJO, topography can also influence diurnal cycle that in turn influences the MJO and atmospheric circulation in the MC. For example, Neale and Slingo (2003) suggested that the regional models with finer horizontal resolutions might capture the diurnal cycle in the MC more accurately than general circulation models (GCMs). This result was further confirmed by Qian (2007), who showed that the inadequate representation of complex topography in the MC produces systematic errors in GCMs compared to the regional models. However, using a cloud-system resolving global model, Miura et al. (2007) captured the amplitude and propagation speed of an MJO event. They found that the higher-resolution led to better representation of topography and SST, which led to better coupling between convection and circulation. Therefore, better representation of topography in the MC is important for MJO simulation (e.g., Takasuka et al. 2015; Wu and Hsu 2009). A more detailed survey of literature on the role of topography on the MJO in the MC can be found in Tseng et al. (2017).

The land-sea contrast provided by the MC islands also plays a key role on MJO propagation (e.g., Qian 2007; Zhang and Ling 2017; Tseng et al. 2017). Using cloud-resolving idealized simulations, Wang and Sobel (2017) showed that when the prevailing winds are weak precipitation is enhanced over the islands due to the dominance of land-sea breezes. For moderate winds, the precipitation tends to be suppressed by the decrease in land-sea temperature contrasts induced by horizontal advection of temperature. When the large-scale winds are strong, gravity waves are crucial for precipitation. Wang and Sobel (2017) concluded that topography up to 800-m does not significantly modify the large-scale flow. Other studies using global climate models (e.g., Tseng et al. 2017) concluded that the MC topography profoundly influences the large-scale winds. However, these studies did not confirm whether such differences are due to the use of different models or simply to the height of the topography.

The importance of topography on MJO and its associated circulation in the MC is receiving progressively more attention. However, numerical models have difficulty in simulating the MJO and its propagation partly because their coarse grid-spacing inadequately represent the complex topography together with problems due to inadequate model physics (e.g., cumulus parameterization). This study uses a high-resolution regional model with sophisticated physics to study the influence of topography on MJO and its propagation in the MC. The objective of the study is to evaluate the role of topography on an MJO event and its dependence on the model resolution. The paper is organized as follows: model, data and simulation design are described in Sect. 2. Section 3 provides results, followed by conclusions and further discussions in Sect. 4.

2 Model, data and simulation design

2.1 Model

Simulations are conducted using the Weather Research and Forecasting (WRF, Skamarock et al. 2008) model version 3.6 over the MC with 41 sigma levels, and 9 levels in the lowest 1 km. The model top is fixed at 10 hPa. All simulations were performed from 0000 UTC, April 1, 2009, to 1800 UTC, April 30, 2009. The frequency of the output is 1 h. We use the following parameterization schemes for this study: Kain–Fritcsh (Kain 2003) scheme for cumulus parameterization; Noah land surface model (Chen and Dudhia 2001) for surface layer parameterization; the rapid radiative transfer model (RRTMG, Iacono et al. 2008) scheme for longwave radiation; the updated Goddard scheme (Chou and Suarez 1994; Shi et al. 2010) for shortwave radiation; the Mellor–Yamada–Janjić (Janjić 1994) scheme for the planetary boundary layer; and the WRF Single Moment 6 (WSM6, Lim and Hong 2010) scheme for microphysics.

The MJO has been simulated successfully by the WRF model previously in a number of studies (e.g., Ray et al. 2011; Hagos et al. 2016; Wang et al. 2015), but most of those studies used coarse resolution simulations. Here, we perform both coarse- and high-resolution simulations over the MC to assess the influence of topography on the MJO and its dependence on the model horizontal resolution. The number and spacing of vertical levels do not change across the simulations. Simulated means were based on the simulation period (April 2009) and the anomalies were calculated after subtracting the mean from the actual values.

2.2 Data

Model initial and boundary conditions are obtained from the ERA-Interim reanalysis (0.25° × 0.25°, 6 h, Dee et al. 2011). The topography and land use data are taken from the 30-s resolution United States Geological Survey (USGS). Precipitation and precipitable water are from the Tropical Rainfall Measuring Mission (TRMM, 0.25° × 0.25°, 3-h, Kummerow et al. 1998) version 3B42 rainfall product and MODIS Level 3 atmospheric products (MOD 08, 1° × 1°, Platnick et al. 2015). All the simulation outputs are averaged daily for comparison and analysis.

2.3 Simulation design

We simulate the passage of a strong (LaFleur et al. 2015) MJO event across the MC, supplemented with sensitivity simulations to quantify the role of topography on the MJO. All the simulations cover the entire MC (80°E–160°E, 20°S–20°N) area and are described in Table 1. The lower resolution (LR) simulation has 12 km horizontal grid-spacing and 794 × 363 horizontal grid points. The higher resolution (HR) simulation has 4 km horizontal grid-spacing and 2145 × 921 horizontal grid points. The integration time step is 60 s for the LR and LR-Flat simulations and 20 s for HR and HR-Flat simulations. All the simulations are conducted for the month of April 2009, when an MJO event crossed the MC (Fig. 2). This time period lies within the Year of Tropical Convection (YOTC, Moncrieff et al. 2012a, b; Waliser et al. 2012).

This MJO event propagated close to the equator and over the MC islands, a typical property of MJO events in the spring season (Zhang and Dong 2004; Ray et.al. 2009; Ray and Zhang 2010). This allows us to quantify the role of topography on the amplitude and propagation of this event. In the boreal winter, when typically strongest, the MJO tends to propagate over the oceanic regions. Based on the real-time multivariate MJO (RMM, Wheeler and Hendon 2004) index, this event entered the MC around April 14–15 and

Table 1 The description of simulations and their purposes

Experiments	Description	Purpose
Lower-resolution (LR)	Simulation with cumulus parameterization	To explore the model's ability to capture the MJO in the MC in lower-resolution simulation
Lower-resolution flat (LR-Flat)	Same as LR, but remove topography in the MC to a unified flat land (2 m)	To explore the role of topography on MJO in a lower-resolution simulation
Higher-resolution (HR)	Same as LR, but with higher horizontal resolution; no cumulus parameterization	To explore the role of higher-resolution simulation
Higher-resolution flat (HR-Flat)	Same as HR, but remove topography in the MC to a unified flat land (2 m); no cumulus parameterization	To explore the role of topography on MJO in a higher-resolution simulation
Lower-resolution flat over New Guinea (LR-Flat-NG)	Same as LR, but remove topography in the New Guinea to a unified flat land (2 m)	To explore the upstream effect of the New Guinea topography

The horizontal resolution is 12 km for LR, LR-Flat, and LR-Flat-NG, and is 4 km for HR and HR-Flat. All simulations were conducted over the MC region (Fig. 1, 80°–160°E, 20°S–20°N) for the month of April, 2009

exited around April 22 (Fig. 2a). This MJO event was an active–active (AA) event (Barrett et al. 2017), i.e., an event that entered the MC in phase 4 with an RMM amplitude greater than 1.0 and maintained an RMM amplitude of 1.0, or greater, as it exited the MC in phase 5. Using reanalysis data from 1980 to 2015, Barrett et al. (2017) found that about 50% of the events that propagate through the MC are in the AA category. Therefore, our chosen MJO event is suitably representative and therefore typical across the MC. Even though the RMM index does not show any decrease in amplitude, the convective and circulation anomalies over the MC decreased according to the longitude-time structures of the ERA-Interim reanalyzed zonal winds at 850 hPa (U850) and TRMM precipitation in Fig. 2b, c, respectively. The zonal wind was predominantly westerly in the lower troposphere and easterly in the upper troposphere in the MC area during the passage of this MJO event. A clear transition of U850 winds from easterlies to westerlies (Fig. 2b) and of precipitation from negative to positive anomalies (Fig. 2c), occurred around April 13–14 at 90°E. The eastward propagation of U850 seems to be smoother than the precipitation, which is interrupted by the presence of land. To the east of 120°E (i.e. east of Borneo), both U850 and precipitation propagated eastward with greater amplitudes in the presence of less land area.

3 Results

3.1 Structure and propagation of the simulated MJO

The LR simulation (Fig. 3a), which uses cumulus parameterization, shows a weak eastward propagation west of 110°E around April 14–15. However, little to no eastward propagation occurs east of 110°E, and seems to be dominated by westward-propagating synoptic-scale systems (e.g., Tulich and Kiladis 2012). Also, there is less precipitation in the adjacent areas to the east of the islands. Such weakening of convection has previously been reported due to orographic blocking of the Kelvin wave embedded in the MJO (e.g., Hsu and Lee 2005; Wu and Hsu 2009; Zhang and Ling 2017) and to influences of the diurnal convective cycle in the MC (e.g., Hagos et al. 2016). Whether the topography had any role in disrupting the MJO associated precipitation is tested by removing the topography (LR-Flat in Table 1). The LR-Flat simulation clearly shows coherent eastward propagation in precipitation (Fig. 3b), implying possible topographic influences on the eastward propagation in precipitation. The LR-Flat simulation results also indicate that in the absence of topography, cumulus parameterization may have the essential physics to capture convection of the MJO (e.g., Dias et al. 2013).

When cumulus parameterization is removed in the high-resolution simulation (HR in Table 1), the eastward propagation (Fig. 3c) is more organized than in the LR simulation (Fig. 3a). The spurious westward-propagating features are also reduced in the HR compared to the LR during April 18–23, indicating an improvement in representing those features in the higher resolution simulation. In particular, the MJO propagation around April 14–15 at 90°E in the observations (Fig. 2c) is fairly well captured by the HR simulation (Fig. 3c). When the topography is removed in the high-resolution simulation (HR-Flat in Table 1), the eastward propagation becomes even more organized (Fig. 3d) compared to the HR (Fig. 3c). Both LR-Flat and HR-Flat simulations, in general, show stronger precipitation than simulations with topography east of 130°E. The similarity of these results indicates that the MJO propagation across the MC is not only dependent on the model resolution but is also influenced by the complex topography and its representation in the simulations.

It is important to also highlight that the simulations with topography (LR and HR) have aspects that disagree

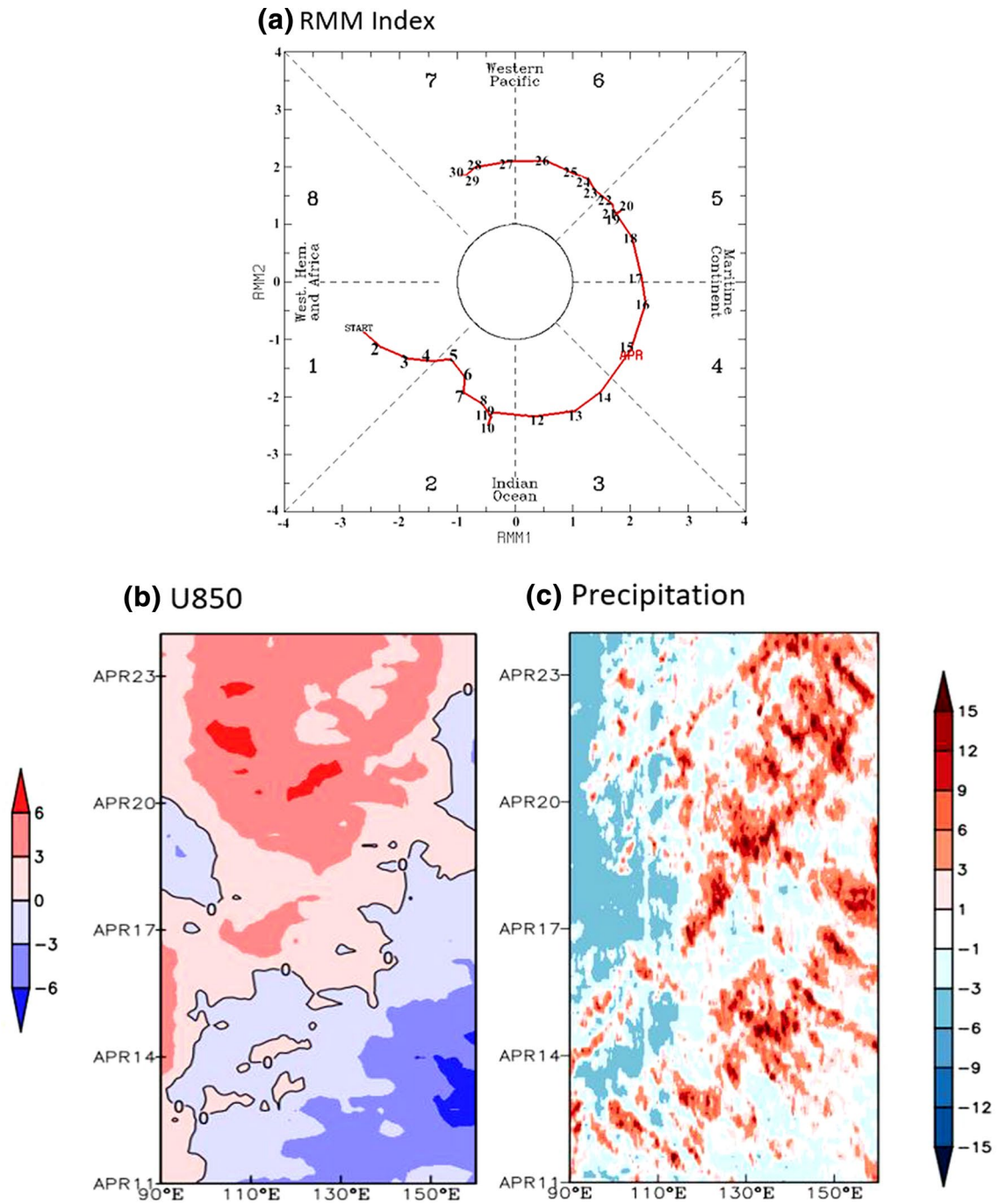

Fig. 2 **a** Progression of this MJO event through the real-time multivariate MJO (RMM) phase space for April 2009. The numbers along the red curve show the dates of MJO propagation. **b** Longitude-time structures of daily anomalies of zonal winds at 850 hPa (U850, m s^{-1}) from the ERA-Interim and **c** TRMM precipitation (mm day^{-1}), both averaged over 10°S–10°N

with reanalysis. For example, the eastward propagation speed of MJO associated precipitation in LR (Fig. 3a) and HR (Fig. 3c) is faster compared to that of the observations (Fig. 2c). Whether this is due to the computational domain of the model that is not big enough to accommodate the Rossby gyres, or due to the lack of air–sea interactions (e.g., Flatau et al. 1997; Sobel et al. 2010) or some other reason, is beyond the scope of this paper.

To further explore the role of topography, we examine the horizontal and vertical structure of the circulation and convection between the simulations with and without topography and observations in Figs. 4, 5 and 6. Figure 4 shows

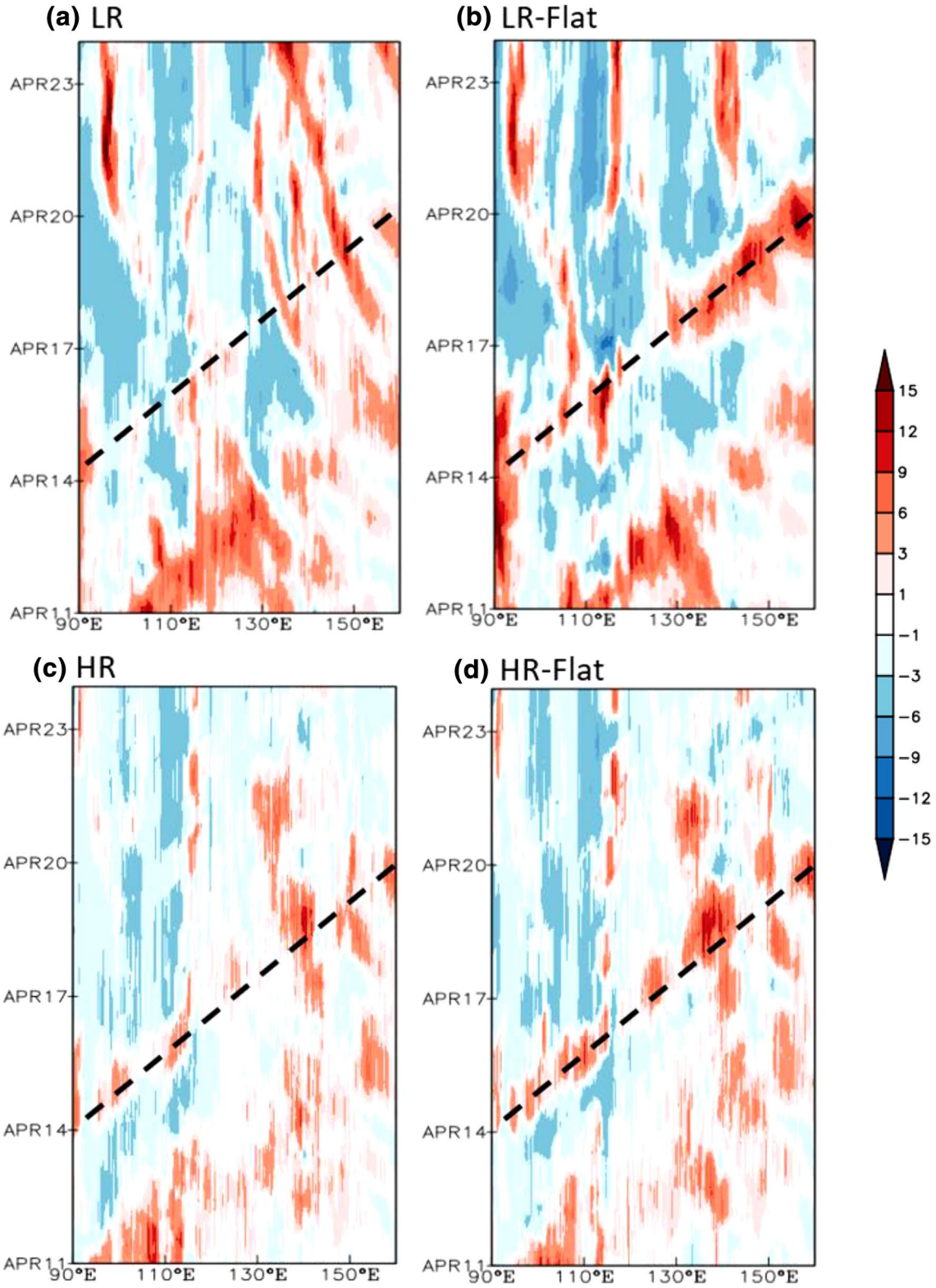

Fig. 3 Time-longitude structures of precipitation anomaly (mm day^{-1}) from the **a** LR, **b** LR-Flat, **c** HR and **d** HR-Flat, averaged over 10°S–10°N. Black dashed lines indicate the MJO propagation

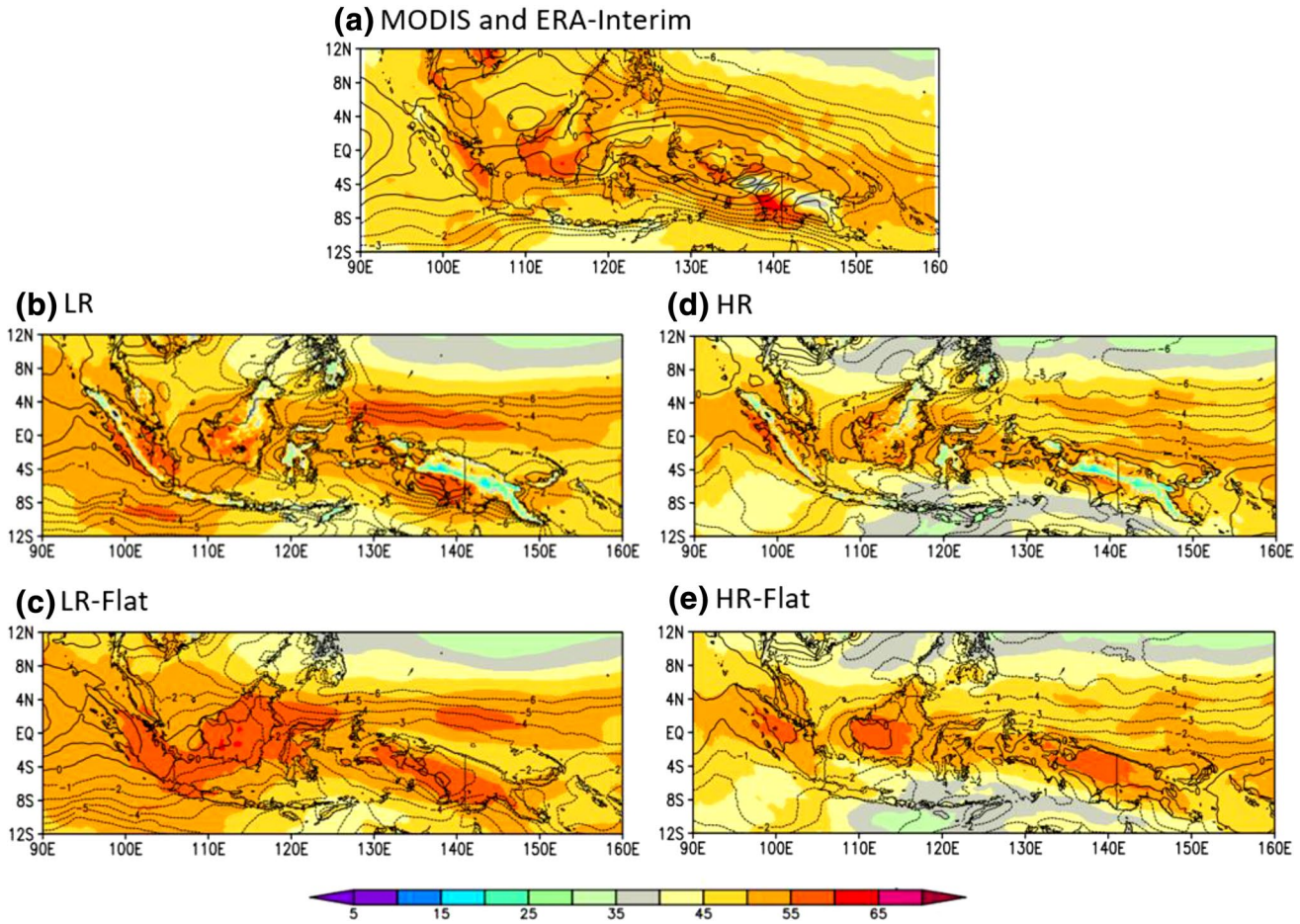

Fig. 4 Precipitable water (mm, shaded) and U850 (m s^{-1}, contour) for April 2009 from **a** observations (MODIS and ERA-Interim), **b** LR, **c** LR-Flat, **d** HR and **e** HR-Flat

precipitable water (PWAT) and zonal winds at 850 hPa. The LR (Fig. 4b) and HR (Fig. 4d) PWAT shows a general agreement with the observations (Fig. 4a), but are drier over the mountains, in particular over New Guinea. Comparisons of LR-Flat with LR shows that without topography, the precipitable water increases over the Sumatra-Borneo region due to stronger easterly winds. The HR-Flat also shows this behavior compared to HR. The mean zonal winds in the ERA-Inerim (Fig. 4a) were fairly well captured by the LR (Fig. 4b) and HR (Fig. 4d). The U850 to the west of Sumatra was better captured by the LR than HR. In general, however, over the rest of the domain, the HR performed better than the LR. In LR-Flat simulations, westerlies are stronger between Sumatra and Borneo. The differences are significantly smaller in high-resolution simulations.

Figure 5 shows the vertical structure of the zonal winds in Area A. The low-level transition of winds from easterly to westerly around April 16 in the reanalysis (Fig. 5a) is well captured by the LR (Fig. 5b) and HR (Fig. 5d). The amplitude of the anomalies is stronger in the LR than the reanalysis around April 16, but is somewhat weaker afterwards. In the absence of topography in low resolution (LR-Flat, Fig. 5c), the westerly flow is deeper and stronger than the LR (Fig. 5b) around April 16. The deep westerly flow between April 21 and April 26 in the reanalysis (Fig. 5a) is better captured by the HR (Fig. 5d) than the LR (Fig. 5b). The first-baroclinic mode structure of zonal winds is evident in all the simulations. The lower-level convergence and upper-level divergence in the ERA-interim (Fig. 5a) around April 28 is better captured by the HR (Fig. 5d) than the LR (Fig. 5b). The results are consistent over other areas.

The influence of topography on the circulation during the passage of the MJO is further discussed in Fig. 6. In the LR-Flat over Area A (Fig. 6b), anomalous westerlies are much stronger than those in the LR (Fig. 6a). The lower troposphere is dominated by the deep vertical structure, with maximum amplitudes around 106°E and 700 hPa. The influence over Area B from LR-Flat (Fig. 6d) compared to LR (Fig. 6c) is also quite evident. The flow is clearly interrupted by the topography over Borneo and Sulawesi leading

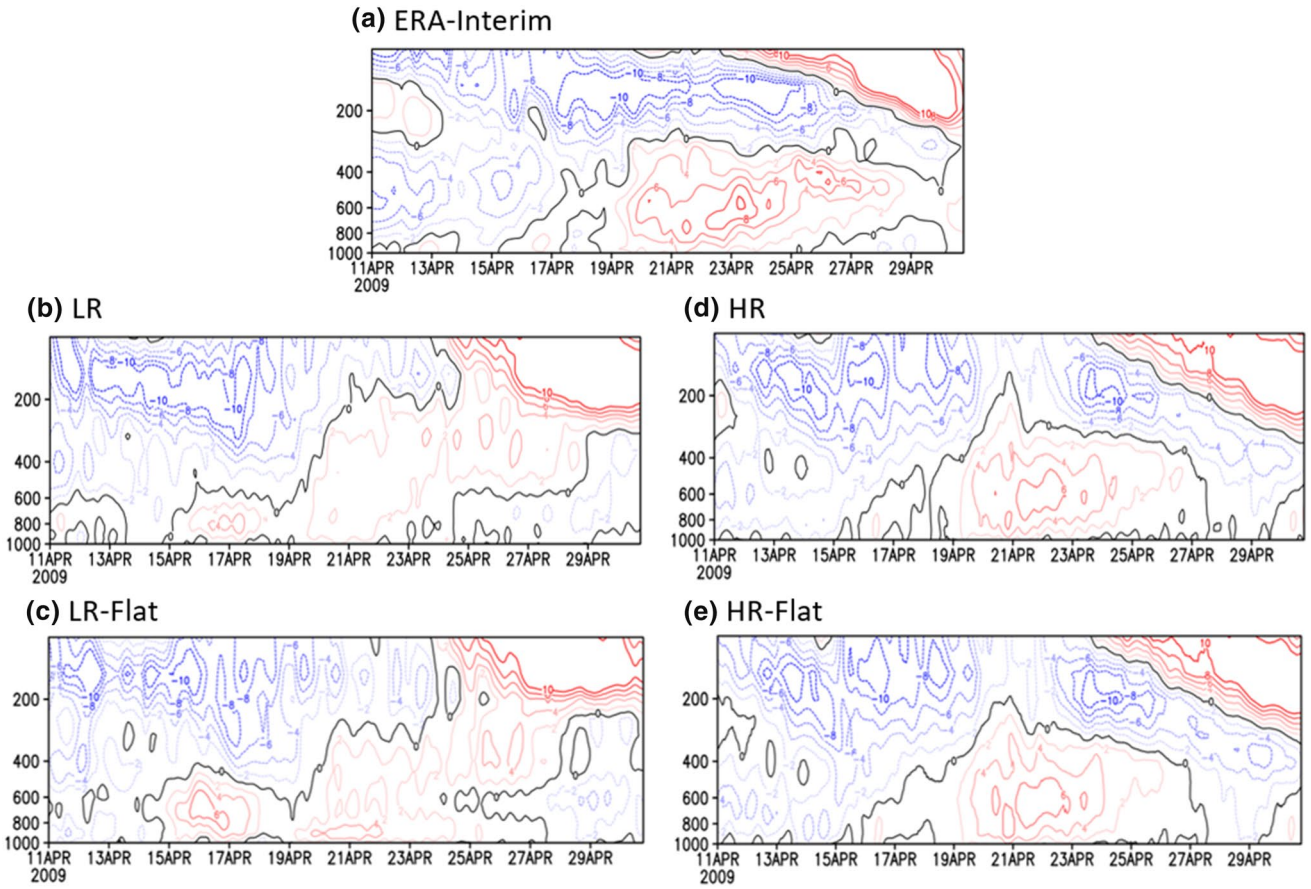

Fig. 5 Time-vertical structure of zonal wind anomalies (contour, m s^{-1}) for Area A from the **a** ERA-Interim, **b** LR, **c** LR-Flat, **d** HR and **e** HR-Flat. Contours are plotted from − 10 to 10 m s^{-1} with an interval of 2

to weaker flow in LR than LR-Flat. Over area C, the effects from the New Guinea mountain range is also evident (not shown).

It is clear that the precipitation anomalies are in general stronger over the ocean to the east of the major islands (Sumatra, Borneo and New Guinea) in the MC during MJO propagation in both Flat simulations, and is particularly evident in the LR-Flat simulation (Fig. 3). Three regions to the east of the islands are chosen for detailed analyses in the next section, and they are shown by the dashed black boxes in Fig. 1a. Area A (105°–111°E, 10°S–10°N) represents the part between Sumatra and Borneo, Area B (122°–128°E, 10°S–10°N) represents east of Borneo and Sulawesi, and Area C (150°–156°E, 10°S–10°N) represents an area east of New Guinea.

3.2 Role of topography

To quantify the role of topography in the MC on the MJO-associated precipitation, we conduct a column-integrated moisture budget (e.g., Hsu and Li 2012; Ray and Li 2013; Wang et al. 2015) analysis using the following equation:

$$\langle \frac{\partial q}{\partial t} \rangle = -\langle v_h \cdot \nabla q \rangle - \langle \omega \frac{\partial q}{\partial p} \rangle + E - P + R \quad (1)$$

where q is the specific humidity, v_h is the horizontal wind vector, ω is the vertical velocity, E is the evaporation, P is the precipitation and R is the residual. In Eq. (1), <> denotes a mass-weighted vertical integral from surface to 100 hPa. The term on the left-hand side represents the moisture tendency. The first and the second terms on the right-hand side are the horizontal (HADV) and vertical advection (VADV), respectively. For the rest of this study, we discuss the three most dominant terms (precipitation, HADV and VADV) since they are much larger than the moisture tendency, evaporation and residual over the three Areas A, B and C.

For Area A, the dominant terms of the moisture budget are shown in Fig. 7. The evaporation and residual terms are not shown here because they are small and vary little across the simulations with and without topography. The MJO propagates across Area A during April 14–16 and is indicated by an increase in anomalous precipitation (Fig. 3). The

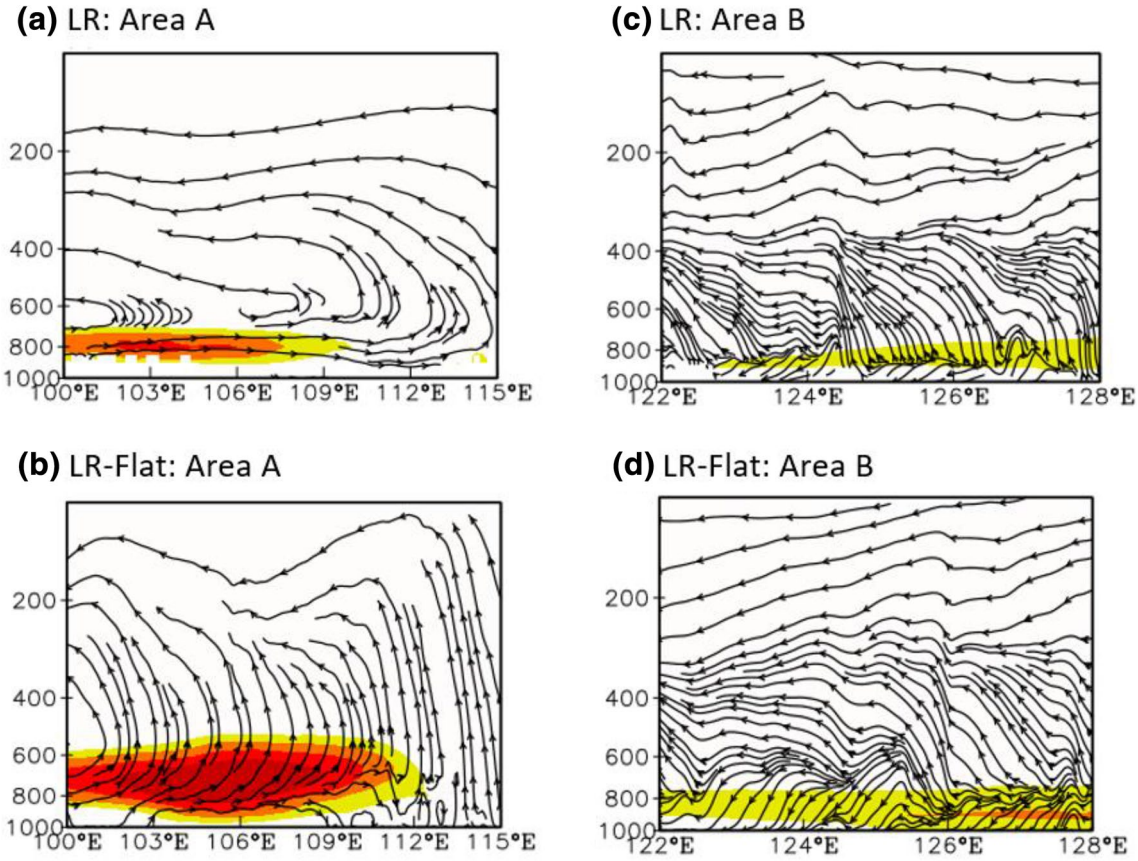

Fig. 6 Vertical cross section of zonal wind anomalies (shaded, m s^{-1}) and mean circulation (stream line) over Area A from **a** LR and **b** LR-Flat. Right panels are over Area B. Shadings are plotted from 2 to 5 m s^{-1} for every 1 m s^{-1}. Vertical motion has been multiplied by 100. The calculation for Area A is for April 14–16 and for Area B is for April 15–17

precipitation over Area A in the LR-Flat increases to a maximum of 10 mm day^{-1}, compared to only about 4 mm day^{-1} in the LR. This increase in precipitation is due to an increase in vertical advection of moisture in the absence of topography (Fig. 7c, red). The change in the horizontal moisture advection is small, and is decreased slightly in the LR-Flat simulation (Fig. 7b). For the HR-Flat simulation, the increase in precipitation compared to the HR simulation (Fig. 7a, light-blue and green) is also due to the increase of the vertical moisture advection (Fig. 7c). Horizontal advection plays a minor role (Fig. 7b). The results indicate that in the absence of topography, the MJO propagates across the MC more coherently due to an increase in vertical moisture advection east of the island. This effect is more pronounced in the LR-Flat case than the HR-Flat case. The amplitude of change in the vertical structure of vertical velocity and humidity are explored later to quantify the relative contribution of their changes on the vertical advection of moisture.

For Area B (Fig. 8), which is located to the east of Borneo, precipitation is lower in LR-Flat than LR (Fig. 8a) during the passage of the MJO. This decrease in precipitation seems to be due to a decrease in VADV (Fig. 8c) even though HADV increases (Fig. 8b). The HADV is also found to be larger in HR-Flat than HR (Fig. 8b) and resembles the results of Kerns and Chen (2013). The HADV term from these simulations will be explored further. Interestingly, precipitation is larger in HR-Flat than HR (Fig. 8a), and is due to an increase in HADV (Fig. 8b) even though VADV decreases (Fig. 8c). For Area C, during the passage of the MJO (April 18–20), precipitation is larger when topography is removed and is mostly due to an increase in vertical advection (not shown), and is similar to Area A. This result again indicates that in the absence of topography, the MJO can propagate across the islands more easily.

The relative contribution of different terms on the moisture budget during the passage of the MJO is summarized in Fig. 9. For Area A (Fig. 9a), the VADV in LR-Flat (5.9 mm day^{-1}, Fig. 9a) is much greater than that in LR (2 mm day^{-1}), but the HADV is slightly smaller. Interestingly, HADV and VADV are similar in magnitude for LR indicating that when the topography is removed, MJO-associated vertical advection increases dramatically over the ocean east of the islands. The results are similar for the high-resolution simulations HR and HR-Flat (Fig. 9d), except that

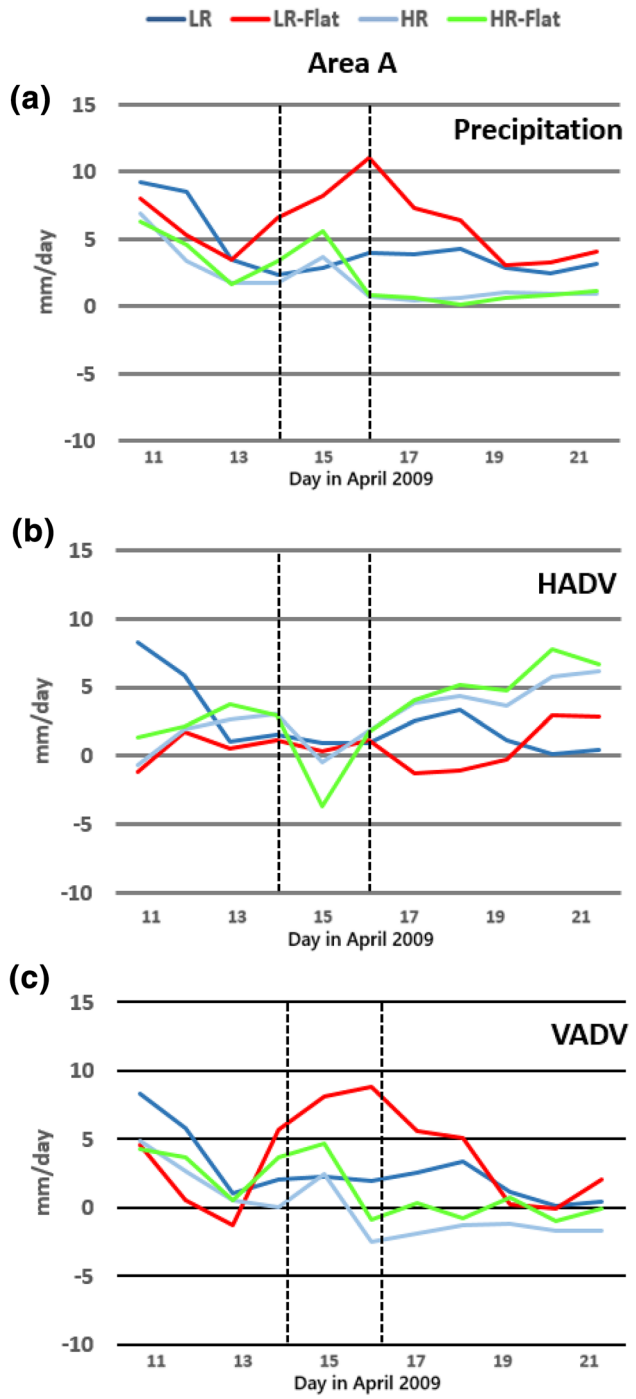

Fig. 7 The three most important terms of the column-integrated tropospheric (1000–100 hPa) moisture budget for Area A (105°–111°E, 10°S–10°N; see Fig. 1a) from the LR (blue), LR-Flat (red), HR (light blue) and HR-Flat (green) simulations. The black dashed lines in each panel represents the time when the MJO propagates across Area A. Unit is in mm day^{-1}

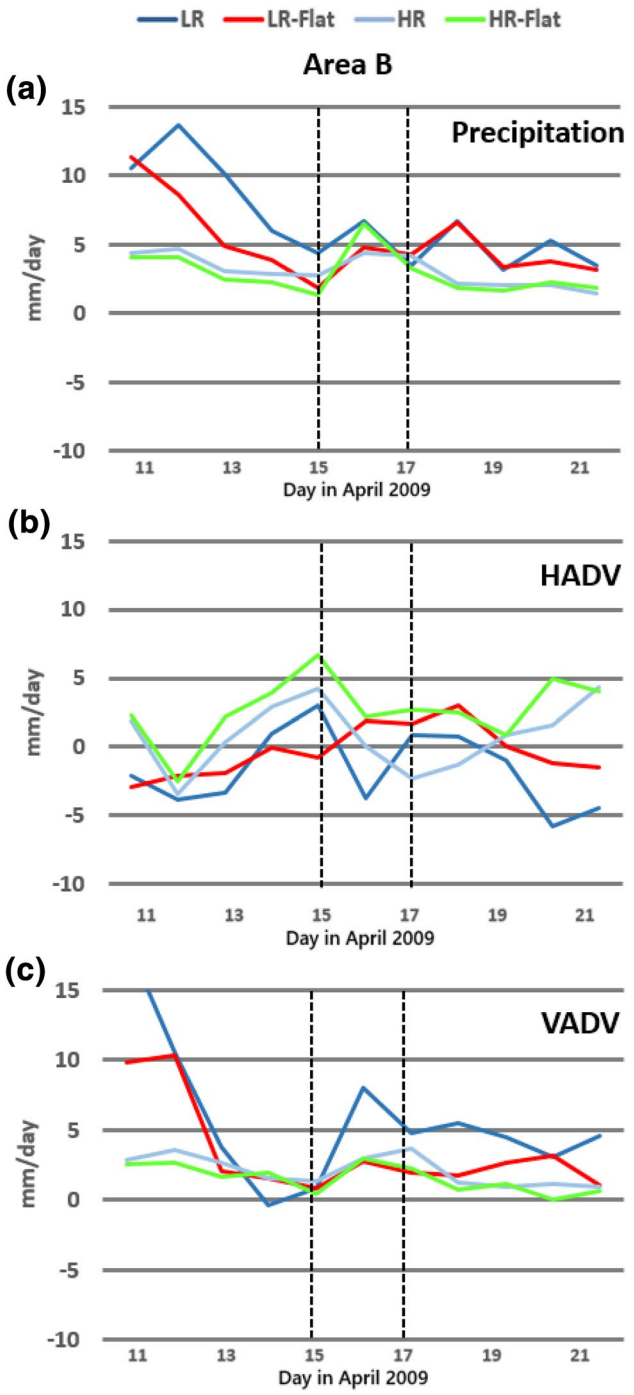

Fig. 8 Same as Fig. 7 but for Area B (122°–128°E, 10°S–10°N; see Fig. 1a)

the changes from HR to HR-Flat are smaller for precipitation and VADV than those from LR to LR-Flat. Horizontal advection in HR-Flat is also reduced compared to HR.

For Area B, which is located east of Borneo, the HADV increase when the topography is removed is evident in both LR-Flat (Fig. 9b) and HR-Flat (Fig. 9e) simulations. This result is different from Area A and Area C, where precipitation increase is balanced by VADV when topography is removed. This difference shows the different behavior of its different parts where the precipitation may be dominated by

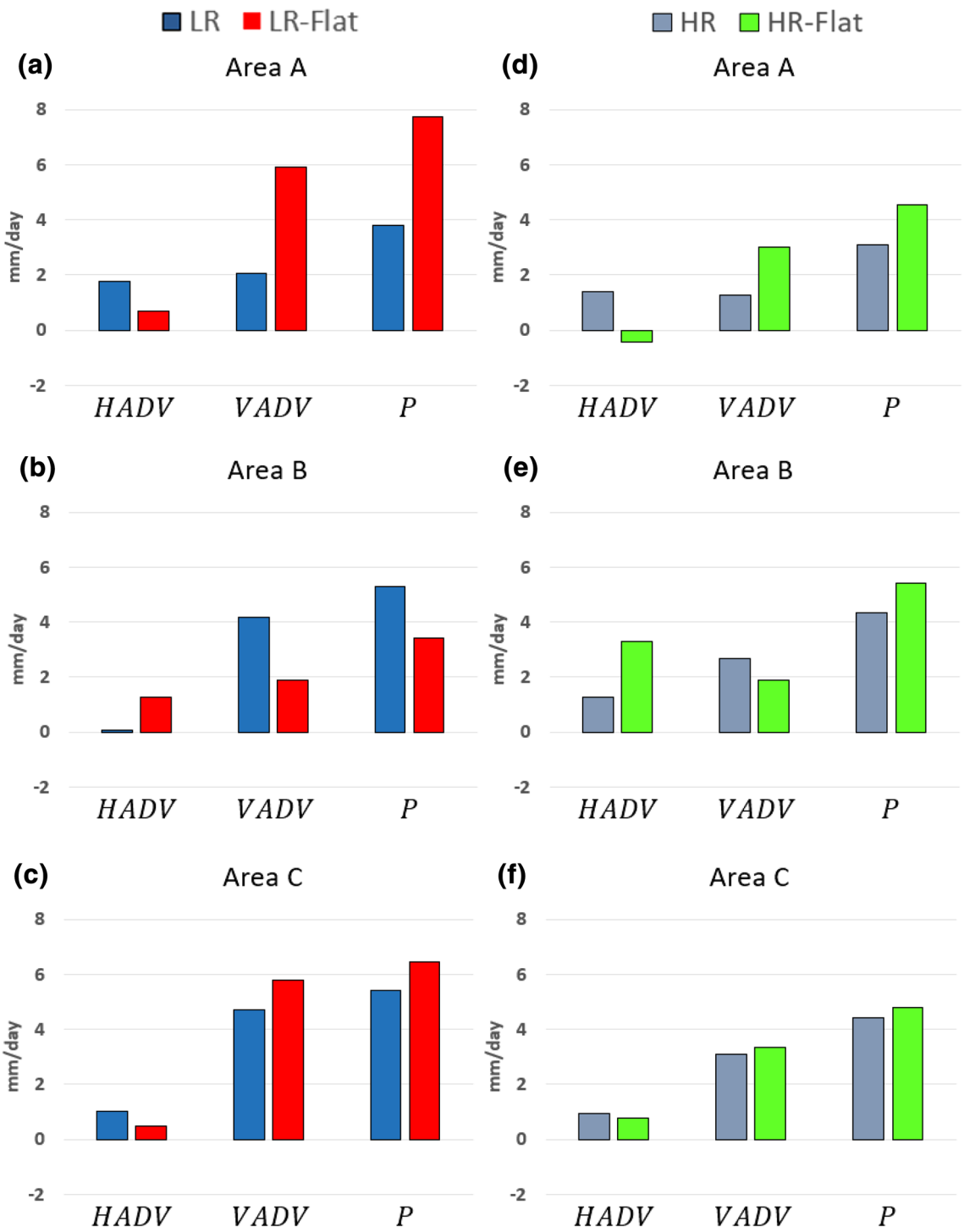

Fig. 9 Left: the column-integrated moisture budget for Area A, Area B, and Area C for LR (blue) and LR-Flat (red). Right panels are for HR and HR-Flat. The terms HADV, VADV and P represents horizontal moisture advection, vertical moisture advection and precipitation, respectively. The MJO propagates through Area A during April 14–16, through Area B during April 15–17 and through Area C during April 18–20 in the model. Units are mm day^{-1}

different processes in. The HADV is higher in LR-Flat (HR-Flat) than LR (HR). The similarity in the relative magnitude of terms in the simulations with different grid-spacings and with and without cumulus parameterization gives confidence to our results and conclusions.

For Area C, during the passage of the MJO, precipitation is greater in the LR-Flat simulation compared to the LR simulation (Fig. 9c), largely due to an increase in VADV, which is consistent with the greater precipitation in LR-Flat than LR in Area A (Fig. 9a). HADV in Area C slightly decreases in the LR-Flat simulation (Fig. 9c) compared to the LR simulation. In the HR-Flat simulation, the increase in precipitation is small compared to the HR (Fig. 9f), possibly because it is located farther from the landmass.

To further explore the increase in vertical advection in the Flat simulations over Area A and Area C, we decompose vertical advection VADV ($\omega\frac{\partial q}{\partial p}$) into four components, $\bar{\omega}\frac{\partial \bar{q}}{\partial p}$, $\bar{\omega}\frac{\partial q'}{\partial p}$, $\omega'\frac{\partial \bar{q}}{\partial p}$, and $\omega'\frac{\partial q'}{\partial p}$. We show results for Area A (Fig. 10) only, since Area C was found to behave similarly. The increase in VADV in LR-Flat compared to Flat (Fig. 10a) is almost entirely due to $\omega'\frac{\partial \bar{q}}{\partial p}$, i.e., advection of mean moisture by the anomalous vertical winds. This is also true for high-resolution simulations (Fig. 10b). Contributions from other components of the VADV are much smaller.

Given the differences in HADV in Area B, the relative contribution of zonal and meridional advection to the HADV over area B is explored further. In Area B, the meridional advection is similar to the zonal advection in LR (Fig. 11a). In the LR-Flat simulation, meridional advection is greater than the LR. In the HR (Fig. 11b) simulation, where topography is better represented, zonal advection is slightly higher than that in the LR. Overall, HADV is larger in the simulations without topography than with topography. For both LR and HR the meridional advection is slightly larger than the zonal advection. However, the change in the zonal advection is larger than the change in the meridional advection when topography is removed. In the HR-Flat, both zonal and meridional advection increase compared to HR leading to an overall

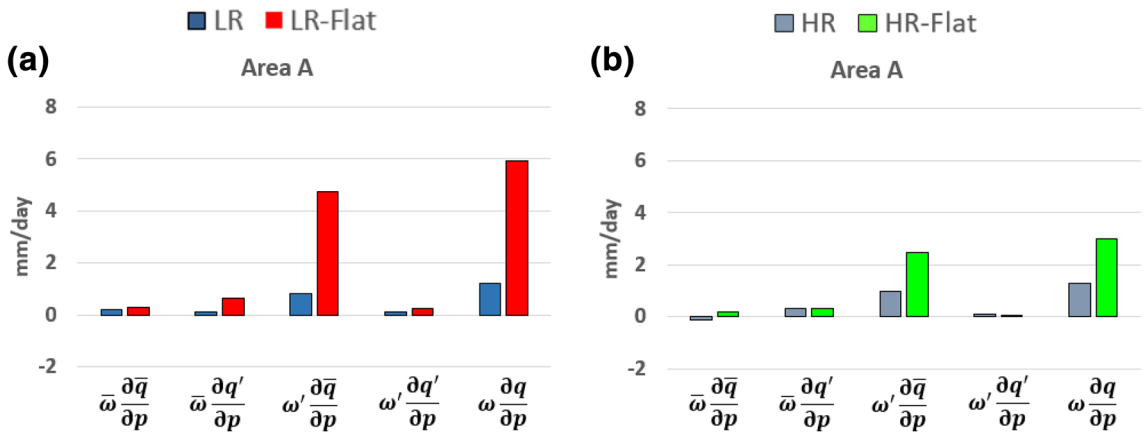

Fig. 10 Top: the components ($\bar{\omega}\frac{\partial \bar{q}}{\partial p}$, $\bar{\omega}\frac{\partial q'}{\partial p}$, $\omega'\frac{\partial \bar{q}}{\partial p}$, $\omega'\frac{\partial q'}{\partial p}$) of column-integrated vertical moisture advection VADV ($\omega\frac{\partial q}{\partial p}$) during April 14–16 in Area A from LR (blue) and LR-Flat (red). Bottom panels are from HR (light blue) and HR-Flat (green). Units are mm day^{-1}

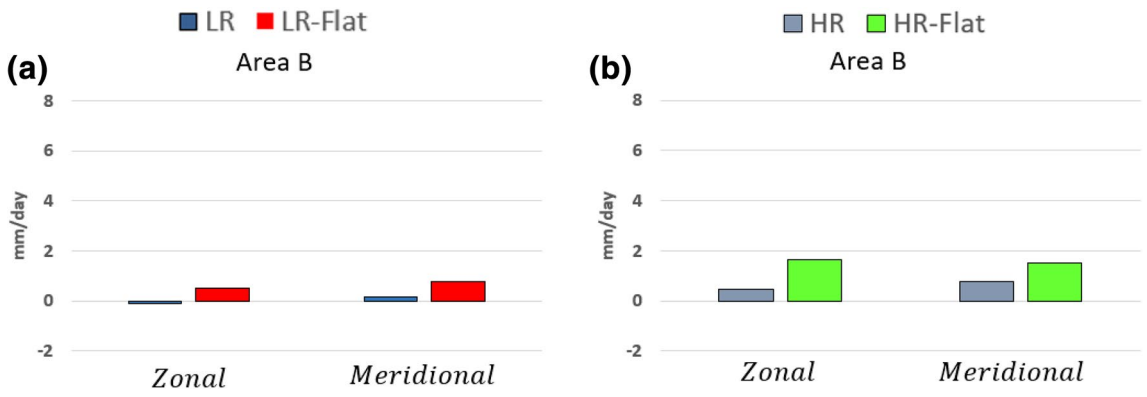

Fig. 11 Left: the column-integrated tropospheric (1000–100 hPa) horizontal moisture advection HADV, separated into zonal and meridional components during April 15–17 in Area B from LR (blue) and LR-Flat (red). Right panel is from HR (light blue) and HR-Flat (green). Units are mm day^{-1}

increase in HADV in HR-Flat. The increase in HADV is consistent in both simulations without topography, and is primarily due to an increase in zonal advection.

To explore the reasons behind the increase in HADV over Area B in Flat simulations, we decompose zonal and meridional advections into four components (Fig. 12). The increase in the zonal advection in the Flat simulations (Fig. 12a, c) is primarily due to an increase in the anomalous moisture advection by the mean zonal winds ($\bar{u}\frac{\partial q'}{\partial x}$). On the other hand, increase in the meridional advection in the LR-Flat compared to LR is due to an increase in the mean moisture advection by the anomalous meridional winds ($v'\frac{\partial \bar{q}}{\partial y}$). The advection of mean moisture by the anomalous meridional winds was also found by Kim et al. (2014).

Figure 13 shows the vertical profile of humidity and vertical velocity for all cases over Area A, Area B and Area C. Between the LR and LR-Flat simulations, the greatest difference in humidity is in the lower and middle troposphere in Area A and Area B, between 800 and 500-hPa (Fig. 13a, b). The maximum difference between LR-Flat and LR in Area A is about 1.5 g kg^{-1} and in Area B is about 1 g kg^{-1}. The removal of topography has very little effect on the humidity over Area C (Fig. 13c), which is farther from the islands. The difference in vertical velocity between LR and LR-Flat is larger over Area A and Area C than Area B. For Area B, the changes in vertical velocity are small from LR to LR-Flat (Fig. 13e). For Area C, the difference between LR and LR-Flat in humidity (Fig. 13c) is small, but for vertical velocity (Fig. 13f) is large, leading to a large change in VADV (Fig. 9c). For high-resolution simulations, the results are similar to the lower resolution simulations, except the

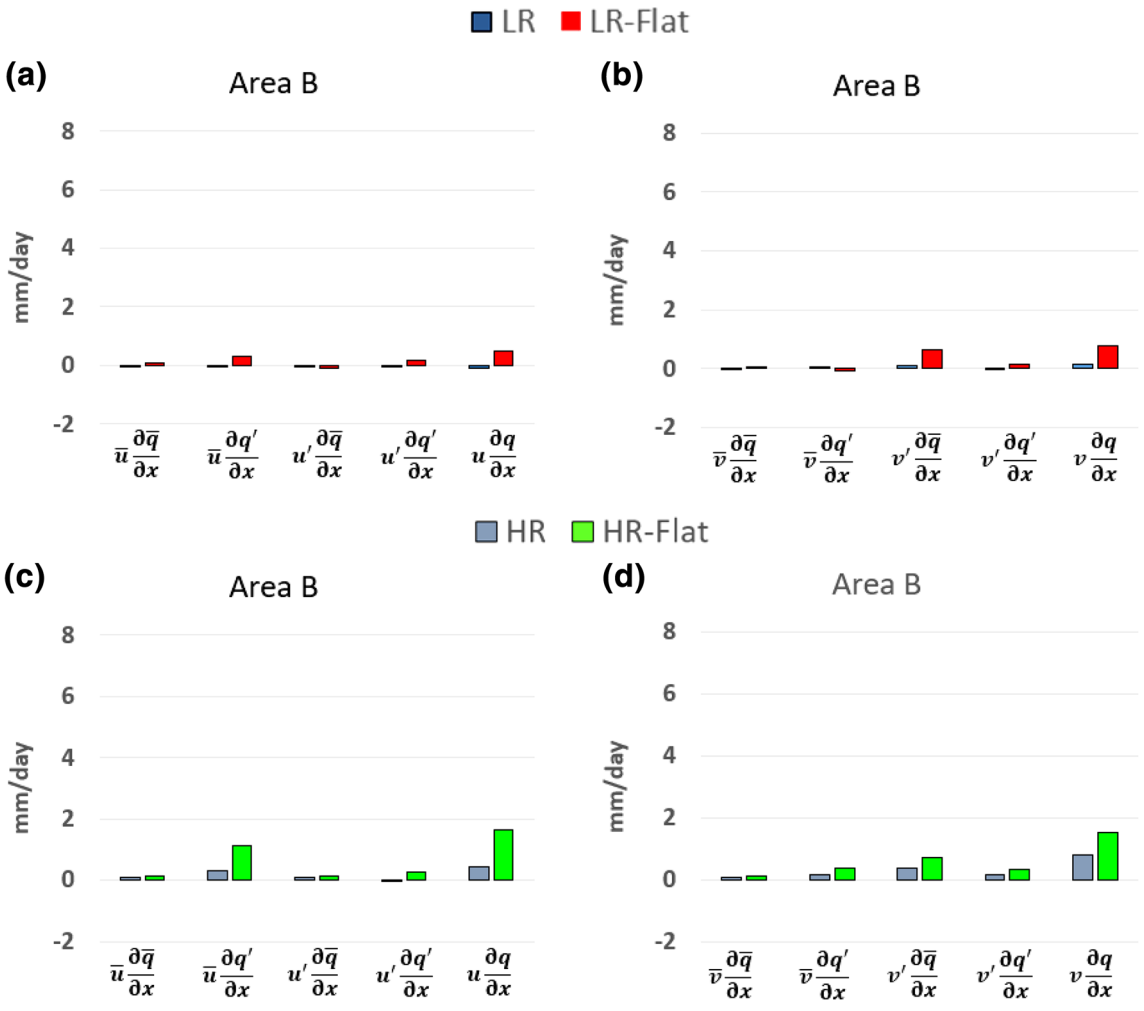

Fig. 12 Left: the column-integrated tropospheric (1000–100 hPa) horizontal moisture advection HADV, separated into 4 zonal components ($\bar{u}\frac{\partial \bar{q}}{\partial x}$, $\bar{u}\frac{\partial q'}{\partial x}$, $u'\frac{\partial \bar{q}}{\partial x}$, and $u'\frac{\partial q'}{\partial x}$; total is $u\frac{\partial q}{\partial x}$) and (right) 4 meridional components ($\bar{v}\frac{\partial \bar{q}}{\partial y}$, $\bar{v}\frac{\partial q'}{\partial y}$, $v'\frac{\partial \bar{q}}{\partial y}$, *and* $v'\frac{\partial q'}{\partial y}$; total is $v\frac{\partial q}{\partial y}$) during April 15–17 in Area B from LR (blue), LR-Flat (red), HR (light blue) and HR-Flat (green). Units are mm day^{-1}

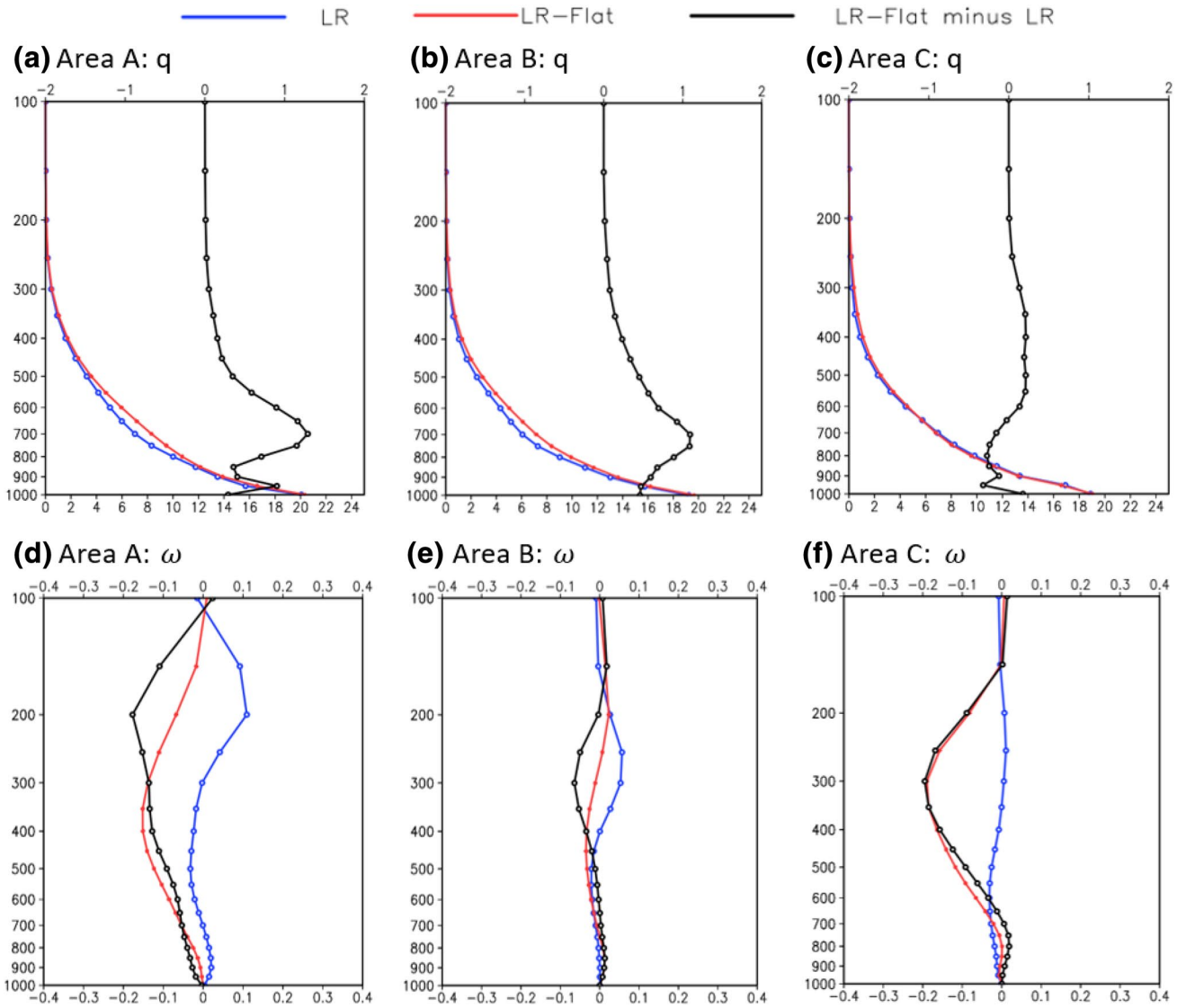

Fig. 13 Top: vertical profile of specific humidity q (g kg^{-1}) from the LR (blue), LR-Flat (red) and LR-Flat minus LR (black) for **a** Area A, **b** Area B and **c** Area C. Bottom panels are for vertical velocity ω (Pa S^{-1}). The black dotted line use top axis

difference between HR and HR-Flat is small leading to a smaller change in VADV (not shown).

Overall, the simulations with lower and higher resolutions are consistent with each other over Area A and Area C. However, over Area B, there is a decrease (increase) in precipitation in LR-Flat (HR-Flat) compared to LR (Fig. 9b, e) due to a decrease in vertical advection. There is a decrease in VADV in HR-Flat also, but the decrease is compensated by a larger increase in HADV leading to an increase in precipitation. Given the complexity of this region, we show the results for another area to the east of Area B (128°–134°E, 10°S–10°N, hereafter B1). Increase in precipitation in LR-Flat (Fig. 14a) and HR-Flat (Fig. 14b) is found to be due to an increase in HADV. The VADV decreases slightly in both cases. The HADV is about 3 (2) times higher in LR-Flat (HR-Flat) than LR (HR). This increase in HADV is found to be due to an increase in zonal advection in Flat simulations (Fig. 14c, d). The changes in the meridional advection were small. The decomposition of zonal advection into four components (Fig. 14e, f) indicates that the increase in the zonal advection in the Flat simulatio is primarily due to an increase in the anomalous moisture advection by the mean zonal winds ($\bar{u}\frac{\partial q'}{\partial x}$).

Based on the moisture budget analysis, Area B, where HADV was dominant was different from Area A and Area C, where VADV was dominant in the absence of topography. To explore whether Area B was affected by the upstream effects of New Guinea, we conduct one more simulation by removing topography over New Guinea (LR-Flat-NG in Table 1). In LR-Flat-NG, the precipitation

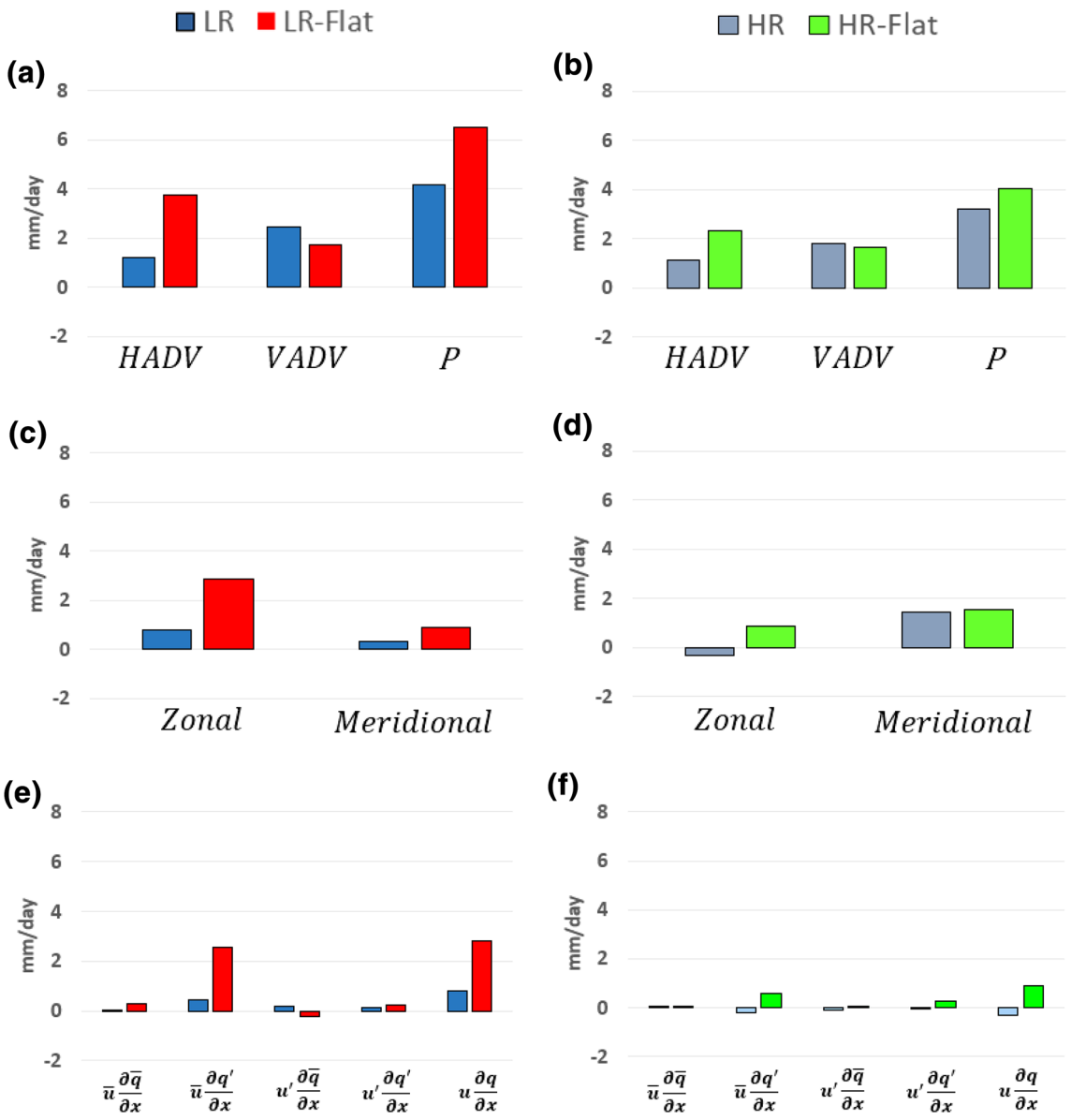

Fig. 14 Left: the column-integrated **a** moisture budget, **b** horizontal moisture advection HADV, separated into zonal and meridional components, and **c** zonal advection, separated into four components ($\bar{u}\frac{\partial \bar{q}}{\partial x}$, $\bar{u}\frac{\partial q'}{\partial x}$, $u'\frac{\partial \bar{q}}{\partial x}$, and $u'\frac{\partial q'}{\partial x}$; total is $u\frac{\partial q}{\partial x}$) for an area to the east of Area B (Area B1, 128°–134°E, 10°S–10°N) from the LR (blue) and LR-Flat (red). Right panels are from the HR (light blue) and HR-Flat (green). The MJO propagates through this Area B1 during April 16–18. Units are mm day^{-1}

increases to the east of 130°E during the passage of the MJO event (Fig. 15). The eastward propagation becomes more coherent in the LR-Flat-NG than LR, which is dominated by westward-propagating synoptic-scale systems. To further explore the upstream effects of the New Guinea topography, we show the moisture budget over Area A and Area B during the passage of the MJO (Fig. 16). For Area A (Fig. 16a), the decrease in precipitation in LR-Flat-NG is primarily due to the decrease of VADV. Change in horizontal advection is small. For Area B (Fig. 16b), the decrease in precipitation is due to the decrease in horizontal advection. As a result, it seems that the increase in HADV in LR-Flat experiment is primarily due to the downstream effects of the islands to the west of Area B. To what extent these results will hold in a high-resolution simulation needs to be investigated in the future.

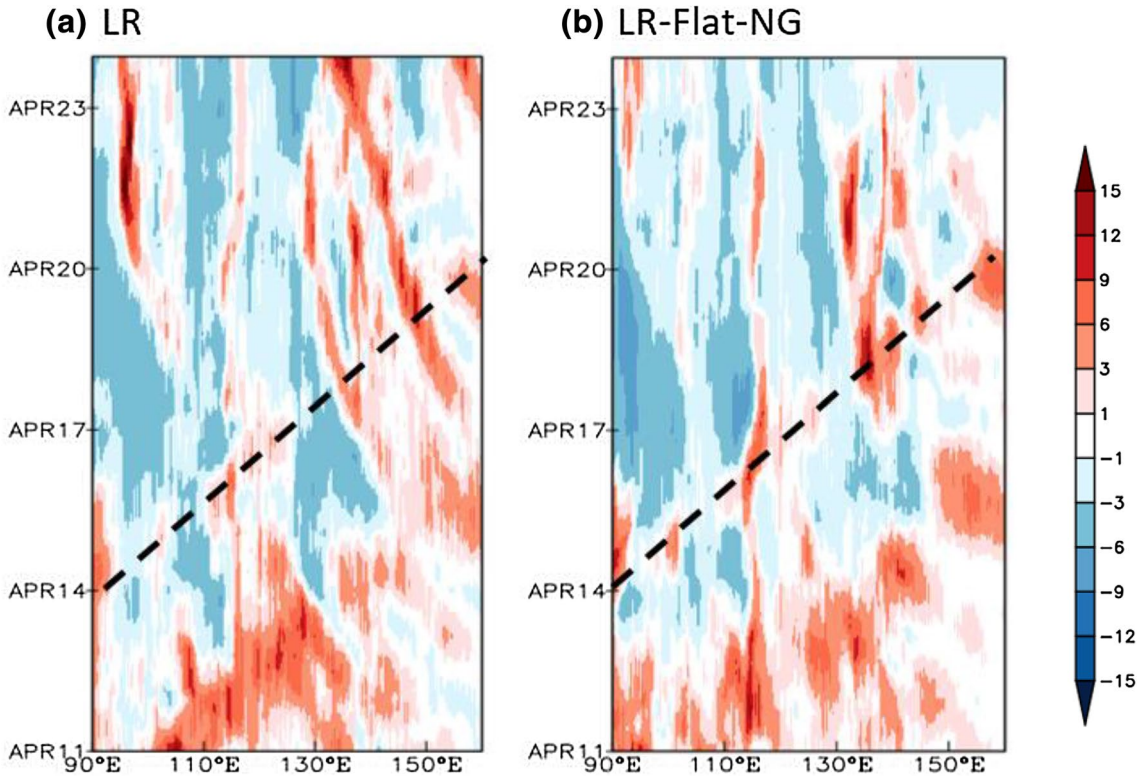

Fig. 15 Longitude-time structures of daily anomalies of precipitation (mm day^{-1}) from the **a** LR and **b** LR-Flat-NG

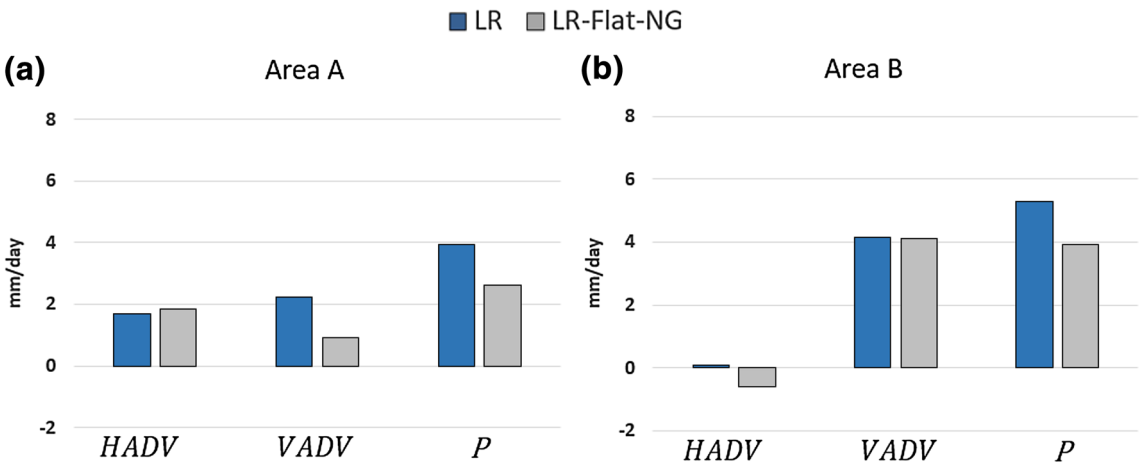

Fig. 16 The column-integrated moisture budget for **a** Area A and **b** Area B from LR and LR-Flat-NG simulations. The terms HADV, VADV and P represents horizontal moisture advection, vertical moisture advection and precipitation, respectively. The MJO propagates through Area A during April 14–16 and through Area B during April 15–17. Units are mm day^{-1}

4 Summary and conclusion

The role of topography (Fig. 1) on a strong MJO event in April 2009 (Fig. 2) in the Maritime Continent is explored using the WRF model. Five simulations are conducted (Table 1): lower resolution (12 km) simulations using cumulus parameterization in the presence (LR) and absence (LR-Flat) of topography, and higher-resolution (4 km) simulations without cumulus parameterization in the presence (HR) and absence (HR-Flat) of topography. A fifth simulation are performed by removing the topography over New Guinea (LR-Flat-NG). In the LR (Fig. 3a), the MJO remains unorganized with no clear eastward

propagation, whereas, in the LR-Flat (Fig. 3b), the simulation captures the MJO and its propagation across the MC. The HR (Fig. 3c) and HR-Flat (Fig. 3d) simulations show several similarities and differences compared to LR and LR-Flat. For example, spurious westward propagating features seen in the LR are reduced substantially in the HR simulation. The MJO is better organized in the Flat simulations than the simulations with topography in both low and high resolutions.

To illustrate the role of topography on the MJO, moisture budget analysis is conducted along the passage of the MJO. In particular, three areas are chosen (Fig. 1a). The Area A (105°–111°E, 10°S–10°N) falls between Sumatra and Borneo; Area B (122°–128°E, 10°S–10°N) is to the east of Borneo and Sulawesi; and Area C (150°–156°E, 10°S–10°N) is to the east of New Guinea. The key finding of this study are:

1. In the absence of topography, vertical advection of moisture is greater to the east of Sumatra and to the eastern edge of the MC, leading to a continuity in MJO associated convection and precipitation compared to the simulations with topography (Figs. 7, 9). The increase in vertical advection in the absence of topography is primarily due to an increase in the mean moisture advection by the anomalous vertical winds (Fig. 10).
2. In the center of the MC (Area B), horizontal advection (Figs. 8, 9) is seemingly important for sustaining the MJO-associated convection in the absence of topography. This indicates the complex nature of the MC, where the dominant physical processes are evidently different for different parts of the region. Further analysis of horizontal advection (HADV) over Area B (Fig. 11) and an area to the east of Area B (Area B1, Fig. 14) shows that the change in zonal advection is dominant in changing the HADV in the Flat simulations compared to the simulations with topography, although the change in meridional advection cannot be ignored during the passage of the MJO. The change in zonal advection is found to be primarily due to the change in anomalous moisture advection be the mean zonal winds (Figs. 12, 14).
3. In the absence of cumulus parameterization, the HR captures the MJO better than LR possibly because the key mesoscale processes are better represented in HR. In the absence of topography, HR-Flat produces slightly higher precipitation to the east of the islands (Fig. 9, right panels). Overall, HR and HR-Flat show several similarities and differences compared to LR and LR-Flat simulations. For example, the vertical advection is stronger in HR-Flat than HR (similar to LR-Flat and LR) except over Area B, but the horizontal advection plays a greater role in high-resolution simulations than low-resolution simulations. The results indicate the sensitivity due to horizontal resolution of the model on the MJO.

There remain some elements, relevant to this study that merit further investigation:

1. Previous studies (e.g., Kim et al. 2017; Zhang and Ling 2017) have demonstrated that most model can reproduce some aspects of the MJO characteristics, but all have some weaknesses representing MJO features like amplitude or propagation across the Maritime Continent (e.g., Slingo et al. 1996; Sperber et al. 1997; Jones et al. 2000). The inability of the numerical models to correctly simulate the MJO and its propagation is primarily thought to be due to their coarse grid-spacings that cannot resolve complex topography and due to inadequate model physics (e.g., cumulus parameterization). In our low-resolution simulation with topography (LR), the model yields less realistic results compared to its high-resolution counterpart (HR). Also, many models that have problems in capturing the MJO propagation across the MC, are able to capture MJO-like disturbances when land is removed (e.g., Ajayamohan et al. 2013; Yoshisaki et al. 2012; Takasuka et al. 2015). Our study shows, at least for the MJO event considered, that topography alone can inhibit MJO propagation in low-resolution simulation using cumulus parameterization
2. We considered one MJO event during the spring season when the MJO is typically closest to the equator (Zhang and Dong 2004). This event was an active–active (AA) event, i.e., an event that entered the MC in phase 4 with an RMM amplitude greater than 1.0 and maintained an RMM amplitude of 1.0 or greater through its exit of the MC in phase 5 (Barrett et al. 2017). Therefore, the extent to which our results may be valid for other MJO events that do not propagate over the MC will be tested later. In particular, previous studies (e.g., Stachnik et al. 2015) have suggested that the propagation of the MJO through the MC might be related to the strength of the MJO itself or to interactions between the MJO convective envelope and other tropical and extratropical wave features. Nevertheless, the case study approach can quantify the physical processes associated with the MJO convection that need to be better observed and understood. Two forthcoming field experiments (Years of the Maritime Continent, YMC; and Propagation of IntraSeasonal Tropical Oscillation, PISTON) are anticipated to provide further insights.
3. Our model has weaknesses in reproducing the MJO rain, and as such, the sensitivity tests based on the LR and HR simulations should be treated with caution. In particular, the possibility that the role of topography on the MJO was overestimated due to poor simulation of the MJO rain in LR cannot be ignored. However, our results are consistent with other studies (e.g., Tseng et al. 2017) where low-resolution simulations with its inadequate

representation of topography combined with the deficiency from cumulus parameterization have difficulty in simulating MJO across the MC.

4. The improvement in the simulated MJO in the HR compared to the LR may come not only from the absence of cumulus parameterization, but also from the better representation of topography in higher resolution simulation. Similarly, the sensitivity of our results to different cumulus parameterizations in the MC on the MJO is not known. These results, however, have shown that in the absence of topography, cumulus parameterization may have the essential physics to capture the MJO in the MC, which is consistent with the conclusions of Dias et al. (2013).

In conclusion, our results show important effects from topography in simulations of the MJO propagation across the MC. The physical processes that are important to the MJO are found to differ in different parts of the MC (our areas A, B, and C), suggesting the presence of additional complexity. We plan to conduct further convection-permitting simulations that resolve mesoscale circulations and more accurately represent complex topography to study the influence of the MC on the MJO and thereby on global weather and climate.

Acknowledgements The simulations were conducted at the Florida Tech using the high-performance computing cluster 'Blueshark', which was funded by the National Science Foundation (NSF). This work was partially supported by Grants from the NSF (1323400) and the ONR (N00014-1601-3091) to PR and ONR (N00014-16WX-01752) to BB. The National Center for Atmospheric Research is sponsored by the NSF.

References

Ajayamohan RS, Khouider B, Majda AJ (2013) Realistic Madden–Julian oscillation initiation and dynamics in a coarse resolution aquaplanet general circulation model. Geophys Res Lett 40:6252–6257. https://doi.org/10.1029/2013GL058187

Barrett BS, Densmore CR, Ray P (2017) Large-scale environmental differences in active and weakening MJO events. J Geophys Res Atmos **(under review)**

Chen F, Dudhia J (2001) Coupling an advanced land surface hydrology model with the Penn State–NCAR MM5 Modeling System. Part I: Model implementation and sensitivity. Mon Weather Rev 129:569–585

Chou MD, Suarez MJ (1994) An efficient thermal infrared radiation parameterization for use in general circulation models. NASA Tech Memo 104606:98. https://pdfs.semanticscholar.org/89b5/ba55c9c4527da0ddaeacce2891605d02cd43.pdf

Dee DP, Uppala SM, Simmons AJ, Berrisford P, Poil P, Kobayashi S, Andrae U, Balmaseda MA, Balsamo G, Bauer P, Bechtold P, Beljaars ACM, van de Berg L, Bidlot J, Bormann N, Delsol C, Dragani R, Fuentes M, Geer AJ, Haimberger L, Healy SB, Hersbach H, Hólm EV, Isaksen L, Kållberg P, Köhler M, Matricardi M. McNally AP, Monge-Sanz BM, Morcrette JJ, Park BK, Peubey C, de Rosnay P, Tavolato C, Thépaut JN, Vitart F (2011) The ERA-interim reanalysis: configuration and performance of the data assimilation system. Q J R Meteorol Soc 137:553–597. https://doi.org/10.1002/qj.828/full

Dias J, Leroux S, Tulich SN, Kiladis GN (2013) How systematic is organized tropical convection within the MJO? Geophys Res Lett 40:1420–1425. https://doi.org/10.1002/grl.50308

Feng J, Li T, Zhu W (2015) Propagating and nonpropagating MJO events over Maritime Continent. J Clim 28:8430–8449. https://doi.org/10.1175/JCLI-D-15-0085.1

Flatau M, Flatau PJ, Phoebus P, Niller PP (1997) The feedback between equatorial convection and local radiative and evaporative processes: the implications for intraseasonal oscillation. J Atmos Sci 54:2373–2386

Hagos S, Zhang C, Feng Z, Burleyson CD, De Mott C, Kerns B, Benedict JJ, Martini MN (2016) The impact of diurnal cycle on the propagation of Madden–Julian oscillation convection across the Maritime Continent. J Adv Mod Ear Syst 8:1552–1564. https://doi.org/10.1002/2016MS000725

Hsu H-H, Lee M-Y (2005) Topographic effect on the eastward propagation and initiation of the Madden–Julian Oscillation. J Clim 18:795–809. https://doi.org/10.1175/JCLI-3292.1

Hsu PC, Li T (2012) Role of the boundary layer moisture asymmetry in causing the eastward propagation of the Madden–Julian Oscillation. J Clim 25:4914–4931. https://doi.org/10.1175/JCLI-D-11-00310.1

Iacono MJ, Delamere JS, Mlawer EJ, Shephard MW, Clough SA, Collins WD (2008) Radiative forcing by longlived greenhouse gases: calculations with the AER radiative transfer models. J Geophys Res 113:D13103. https://doi.org/10.1029/2008JD009944/full

Ichikawa H, Yasunari T (2006) Time-space characteristics of diurnal rainfall over Borneo and surrounding oceans as observed by TRMM-PR. J Clim 19:1238–1260. https://doi.org/10.1175/JCLI3714.1

Ichikawa H, Yasunari T (2008) Intraseasonal variability in diurnal rainfall over New Guinea and the surrounding oceans during austral Summer. J Clim 21:2852–2868. https://doi.org/10.1175/2007JCLI1784.1

Inness PM, Slingo JM (2006) The interaction of the Madden–Julian oscillation with the Maritime Continent in a GCM. Q J R Meteorol Soc 132:1645–1667. https://doi.org/10.1256/qj.05.102

Inness PM, Slingo JM, Guilyardi E, Cole J (2003) Simulation of the Madden–Julian Oscillation in a coupled general circulation model. Part II: The role of the basic state. J Clim 16:365–382

Janjić ZI (1994) The step-mountain eta coordinate model: further developments of the convection, viscous sublayer, and turbulence closure schemes. Mon Weather Rev 122:927–945

Jones C, Waliser DE, Schemm JKE, Lau WKM (2000) Prediction skill of the Madden–Julian oscillation in dynamical extended range forecasts. Clim Dyn 16:273–289

Kain JS (2003) The Kain–Fritsch convective parameterization: an update. J Appl Meteorol 43:170–181

Keenan TD, Carbone RE (2008) Propagation and diurnal evolution of warm season cloudiness in the Australian and Maritime Continent region. Mon Weather Rev 136:973–994. https://doi.org/10.1175/2007MWR2152.1

Keenan TD, Manton MJ, Holland GJ (1989) The island thunderstorm experiment (ITEX)—a study of tropical thunderstorm in the Maritime Continent. Bull Am Meteorol Soc 70(2):152–159

Kerns BW, Chen SS (2013) Cloud clusters and tropical cyclogenesis: developing and nondeveloping systems and their large-scale environment. Mon Weather Rev 141:192–210. https://doi.org/10.1175/MWR-D-11-00239.1

Kim D, Kug J-S, Sobel AH (2014) Propagating versus nonpropagating Madden–Julian Oscillation events. J Clim 27:111–125. https://doi.org/10.1175/JCLI-D-13-00084.1

Kim D, Kim H, Lee MI (2017) Why does the MJO detour the Maritime Continent during austral summer? Geophys Res Lett 44:2579–2587. https://doi.org/10.1002/2017GL072643/

Kummerow C, Simpson J, Thiele O, Barnes W, Chang ATC, Stocker E, Adler RF, Hou A, Kakar R, Wentz F, Ashcroft P, Kozu T, Hong Y, Okamoto K, Iguchi T, Kuroiwa H, Im E, Haddad Z, Huffman G, Ferrier B, Olson WS, Zipser E, Smith EA, Wilheit TT, North G, Krishnamurti T, Nakamura K (1998) The status of the tropical rainfall measuring mission (TRMM) after two years in orbit. J Appl Meteorol 122:1965–1968

LaFleur DM, Barrett BS, Henderson GR (2015) Some climatological aspects of the Madden–Julian Oscillation (MJO). J Clim 28:6039–6053. https://doi.org/10.1175/JCLI-D-14-00744.1

Lim KSS, Hong SY (2010) Development of an effective double-moment cloud microphysics scheme with prognostic cloud condensation nuclei (CCN) for weather and climate models. Mon Weather Rev 138:1587–1612. https://doi.org/10.1175/2009MWR2968.1

Madden RA, Julian PR (1971) Detection of a 40–50 day oscillation in the zonal wind of the tropical pacific. J Atmos Sci 28:702–708

Meehl GA (1987) The tropics and their role in the global circulation system. Geograph J 153:21–36. https://doi.org/10.2307/634469

Miura H, Satoh M, Nasuno T, Noda AT, Oouchi K (2007) A Madden–Julian Oscillation event realistically simulated by a global cloud-resolving model. Science 318:1763–1765. https://doi.org/10.1126/science.1148443

Moncrieff MW, Waliser DE, Miller MJ, Shapiro MA, Asrar GR, Caugley J (2012a) Multiscale convective organization and the YOTC virtual global field campaign. Bull Am Meteorol Soc:1171–1187. https://doi.org/10.1175/BAMS-D-11-002333.1

Moncrieff MW, Waliser DE, Caugley J (2012b) Progress and direction in tropical convection research, YOTC international science symposium. Bull Am Meteorol Soc. https://doi.org/10.1175/BAMS-D-11-00253.1

Mori S, Hamada JI, Tauhid YI, Yamanaka MD, Okamato N, Murata F, Sakurai N, Hashiguchi H, Sribimawati T (2004) Diurnal land-sea rainfall peak migration over Sumatra island, Indonesian Maritime Continent, observed by TRMM satellite and intensive rawinsonde soundings. Mon Weather Rev 132:2021–2039

Neale RB, Slingo JM (2003) The Maritime Continent and its role in the global climate: a GCM study. J Clim 16:834–848

Oh J-H, Kim B-M, Kim K-Y, Song H-J, Lim G-H (2013) The impact of the diurnal cycle on the MJO over the Maritime Continent: a modeling study assimilating TRMM rain rate into Global analysis. Clim Dyn 40:893–911. https://doi.org/10.1007/s00382-012-1419-8

Peatman SC, Matthews AJ, Stevens DP (2014) Propagation of the Madden–Julian Oscillation through the Maritime Continent and scale interaction with the diurnal cycle of precipitation. Q J R Metereol Soc 140:814–825. https://doi.org/10.1007/s00382-012-1419-8

Peatman SC, Matthews AJ, Stevens DP (2015) Propagation of the Madden–Julian Oscillation and scale interaction with the diurnal cycle in a high-resolution GCM. Clim Dyn 45:2901–2918

Platnick S, Hubanks P, Meyer K, King MD (2015) MODIS atmosphere L3 monthly product (08_L3). NASA MODIS Adaptive Processing System, Goddard Space Flight Center

Qian JH (2007) Why precipitation is mostly concentrated over islands in the Maritime Continent. J Atmos Sci 65:1428–1441. https://doi.org/10.1175/2007JAS2422.1

Ramage CS (1968) Role of a tropical "Maritime Continent" in the atmospheric circulation. Mon Weather Rev 96:365–370

Ray P, Li T (2013) Relative roles of circumnavigating waves and extratropics on the MJO and its relationship with the mean state. J Atmos Sci 70:876–893. https://doi.org/10.1175/JAS-D-12-0153.1

Ray P, Zhang C (2010) A case study of the mechanics of extratropical influence on the initiation of the Madden–Julian Oscillation. J Atmos Sci 67:515–528. https://doi.org/10.1175/2009JAS3059.1

Ray P, Zhang C, Dudhia J, Chen SS (2009) A numerical case study on the initiation of the Madden–Julian Oscillation. J Atmos Sci 66:310–331. https://doi.org/10.1175/2008JAS2701.1

Ray P, Zhang C, Moncrieff MW, Dudhia J, Caron JM, Leung R, Bruyere C (2011) Role of the atmospheric mean state on the initiation of the Madden–Julian Oscillation in a tropical channel Model. Clim Dyn 36:161–184. https://doi.org/10.1007/s00382-010-0859-2

Rui H, Wang B (1990) Development characteristics and dynamics structure of tropical intraseasonal convection anomalies. J Atmos Sci 47(3):357–379

Shi JJ, Tao WK, Matsui T, Cifelli R, Hou A, Lang S, Tokay A, Wang NY, Peters-Lidard C, Skofronick-Jackson G, Rutledge S, Petersen W (2010) WRF simulations of the 20–22 January 2007 snow events over eastern Canada: comparison with in situ and satellite observations. J Appl Meteorol 49:2246–2266. https://doi.org/10.1175/2010JAMC2282.1

Skamarock WC et al (2008) A description of the advanced research WRF version3, NCAR Tech, Note NCAR/TN-475 + STR. Natl. Cent. For Atmos Res., Boulder, p 125

Slingo et al (1996) Intraseasonal oscillation in 15 atmospheric general circulation models: results from an AMIP diagnostic subproject. Clim Dyn 12:325–357

Sobel AH, Maloney ED, Bellon G, Frierson DM (2010) Surface fluxes and tropical intraseasonal variability: a reassessment. J Adv Model Ear Syst 2:2. https://doi.org/10.3894/JAMES.2010.2.2

Sperber KR, Slingo JM, Inness PM, Lau WKM (1997) On the maintenance and initiation of the intraseasonal oscillation in the NCEP/NCAR reanalysis and in the GLA and UKMO AMIP simulations. Clim Dyn 13:769–795

Stachnik JP, Waliser DE, Majda AJ (2015) Precursor environmental conditions associated with the termination of Madden–Julian Oscillation events. J Atmos Sci 72:1908–1931. https://doi.org/10.1175/JAS-D-14-0254.1

Takasuka D, Miyakawa T, Satoh M, Miura H (2015) Topographical effects on internally produced MJO-like disturbances in an aqua-planet version of NICAM. SOLA 11:170–176

Tseng W-L, Hsu H-H, Keenlyside N, Chang C-WJ, Tsuang B-J, Tu C-Y, Jiang L-C (2017) Effects of surface orography and land-sea contrast on the Madden–Julian Oscillation in the Maritime Continent: a numerical study using ECHAM5-SIT. J Clim. https://doi.org/10.1175/JCLI-D-17-0051.1 **(in press)**

Tulich SN, Kiladis GN (2012) Squall lines and convectively coupled gravity waves in the tropics: why do most cloud systems propagate westward? J Atmos Sci 69:2995–3012. https://doi.org/10.1175/JAS-D-11-0297.1

Waliser DE, Moncrieff MW, Burridge D, Fink AH, Gochis D, Goswami BN, Guan B, Harr P, Heming J, Hsu H-H, Jakob C, Janiga M, Johnson R, Jones S, Knippertz P, Marengo J, Nguyen H, Pope M, Serra Y, Thorncroft C, Wheeler M, Wood R, Yuter S (2012) The "Year" of Tropical Convection (May 2008 to April 2010): climate variability and weather highlights. Bull Am Meteorol Soc 93:1189–1218. https://doi.org/10.1175/2011BAMS3095.1

Wang S, Sobel AH (2017) Factors controlling rain on small tropical islands: diurnal cycle, large-scale wind speed, and topography. J Atmos Sci 74:3515–3532. https://doi.org/10.1175/JAS-D-16-0344.1

Wang W, Huang M-P, Weaver SJ, Kumar A, Fu X (2014) MJO prediction in the NCEP climate forecast system version 2. Clim Dyn 42:2509–2520. https://doi.org/10.1007/s00382-013-1806-9

Wang S, Sobel AH, Zhang F, Sun YQ, Yue Y, Zhou L (2015) Regional simulation of the October and November MJO events observed during the CINDY/DYNAMO field campaign at gray zone

resolution. J Clim 28:2097–2119. https://doi.org/10.1175/JCLI-D-14-00294.1

Wheeler MC, Hendon HH (2004) An all-season real-time multivariate MJO index: development of an index for monitoring and prediction. Mon Weather Rev 132:1917–1932

Wu CH, Hsu HH (2009) Topographic influence on the MJO in the Maritime Continent. J Clim 22:5436–5437. https://doi.org/10.1175/2009JCLI2825.1

Yang GY, Slingo J (2001) The diurnal cycle in the tropics. Mon Weather Rev 129:784–801

Yoshisaki M, Iga S, Satoh M (2012) Eastward propagation property of large-scale precipitation systems simulated in the coarse-resolution NICAM and an explanation of its formation. SOLA 8:21–24

Zhang C (2005) Madden–Julian Oscillation. Rev Geophys 43:RG2003. https://doi.org/10.1029/2004RG000158

Zhang C, Dong M (2004) Seasonality in the Madden–Julian Oscillation. J Clim 17:3169–3180

Zhang C, Ling J (2017) Barrier effect of the Indo-Pacific Maritime Continent on the MJO: perspectives from tracking MJO precipitation. J Clim 30:3439–3459. https://doi.org/10.1175/JCLI-D-16-0614.1